Preclinical PET Study of Intravitreal Injections

Anxo Fernández-Ferreiro,[1–4] Andrea Luaces-Rodríguez,[1] Pablo Aguiar,[3,5] Juan Pardo-Montero,[3,6] Miguel González-Barcia,[2,4] Lara García-Varela,[3] Michel Herranz,[3,7] Jesús Silva-Rodríguez,[3] María Gil-Martínez,[8] María A. Bermúdez,[9] Alba Vieites-Prado,[10] José Blanco-Méndez,[1] María Jesús Lamas,[2,4] Francisco Gómez-Ulla,[8,11] Álvaro Ruibal,[3,5,12] Francisco Javier Otero-Espinar,[1] and Francisco González[8,11]

[1]Department of Pharmacology, Pharmacy and Pharmaceutical Technology and Industrial Pharmacy Institute, Faculty of Pharmacy, University of Santiago de Compostela, Santiago de Compostela, Spain
[2]Pharmacy Department, Complejo Hospitalario Universitario de Santiago (SERGAS), Santiago de Compostela, Spain
[3]Molecular Imaging Group, Complejo Hospitalario Universitario de Santiago (SERGAS), Health Research Institute of Santiago de Compostela (IDIS), Santiago de Compostela, Spain
[4]Clinical Pharmacology Group, Complejo Hospitalario Universitario de Santiago (SERGAS), Health Research Institute of Santiago de Compostela (IDIS), Santiago de Compostela, Spain
[5]Molecular Imaging Group, Department of Radiology, Faculty of Medicine, University of Santiago de Compostela, Spain
[6]Medical Physics Department, Complejo Hospitalario Universitario de Santiago (SERGAS), Santiago de Compostela, Spain
[7]Galician PET Radiopharmacy Unit, Galaria, Complejo Hospitalario Universitario de Santiago (SERGAS), Santiago de Compostela, Spain
[8]Service of Ophthalmology, Complejo Hospitalario Universitario de Santiago (SERGAS), Health Research Institute of Santiago de Compostela (IDIS), Santiago de Compostela, Spain
[9]Department of Animal Biology, Vegetal Biology and Ecology, Faculty of Biology, University of A Coruña, A Coruña, Spain
[10]Clinical Neurosciences Research Laboratory, Complejo Hospitalario Universitario de Santiago (SERGAS), Health Research Institute of Santiago de Compostela (IDIS), Santiago de Compostela, Spain
[11]Department of Surgery, University of Santiago de Compostela (CIMUS), Spain
[12]Nuclear Medicine Department, Complejo Hospitalario Universitario de Santiago (SERGAS), Santiago de Compostela, Spain

Correspondence: Francisco González, CIMUS, P0, D4, Universidad de Santiago de Compostela, Avd. Barcelona 22, E-15782 Santiago de Compostela, Spain; francisco.gonzalez@usc.es.
Francisco Javier Otero-Espinar, Faculty of Pharmacy, University of Santiago de Compostela, (USC) Pharmacy and Pharmaceutical Technology Department, Praza Seminario de Estudos Galegos s/n E-1570 Santiago de Compostela, Spain; francisco.otero@usc.es.

AF-F and AL-R contributed equally to the work presented here and should therefore be regarded as equivalent authors.

Submitted: March 6, 2017
Accepted: April 26, 2017

Citation: Fernández-Ferreiro A, Luaces-Rodríguez A, Aguiar P, et al. Preclinical PET study of intravitreal injections. *Invest Ophthalmol Vis Sci*. 2017;58:2843–2851. DOI:10.1167/iovs.17-21812

Purpose. This work aimed at describing the time course of vitreous clearance through the use of positron emission tomography (PET) as a noninvasive tool for pharmacokinetic studies of intravitreal injection.

Methods. The pharmacokinetic profile of intravitreal injections of molecules labeled with ^{18}Fluorine (^{18}F) was evaluated in adult Sprague Dawley rats by using a dedicated small-animal PET/computed tomography scanner. Different conditions were studied: three molecules radiolabeled with ^{18}F (^{18}F-FDG, ^{18}F-NaF, and ^{18}F-Choline), three volumes of intravitreal injections (7, 4, and 2 μL), and absence or presence of eye inflammation (uveitis).

Results. Our results showed that there are significant pharmacokinetic differences among the radiolabeled molecules studied but not among the injected volumes. The presence or absence of uveitis was an important factor in vitreous clearance, since the elimination of the drug was clearly increased when this condition is present.

Conclusions. Intravitreal pharmacokinetic studies based on the use of dedicated PET imaging can be of potential interest as noninvasive tools in ophthalmic drug development in small animals.

Keywords: intravitreal injection, radiolabeled molecules, vitreous clearance, intravitreal pharmacokinetics, PET

To date, most topical and systemic drugs have not achieved adequate therapeutic levels in the vitreous, mainly owing to the existence of different physiological barriers.[1] On one hand, topically instilled drugs are diluted by the tear film, thus causing significant drug loss in the lachrymal flow,[2] and furthermore their physicochemical characteristics must be adequate to cross the cornea.[3] On the other hand, the blood–retinal barrier (BRB), which comprises the retinal pigment epithelium and the tightly sealed walls of the retinal capillaries, complicates the arrival of systemic drugs to the vitreous.[4] For these reasons,

intravitreal administration has become an effective way to deliver drugs to the vitreous cavity, allowing high drug concentrations.[5]

To achieve a sustained therapeutic drug concentration in the vitreous, the frequency of administration should be based on the half-life of the drug ($t_{1/2}$). Regarding this question, several in vitro models have been proposed for the study of intravitreal pharmacokinetics, which take into account all aspects of the ocular anatomy and physiology.[6–9] However, one aspect that should be taken into consideration in the in vitro pharmacokinetic studies is the absence of convection,[10–13] even though the principal mechanism of transport through the vitreous is diffusion, and convection does not play a relevant role in the kinetics of small molecules. Other issues such as protein binding, melanin binding, drug metabolism, or active transport are usually not taken into account in the in vitro studies.[8,14] On the other hand, in vivo classical pharmacokinetic studies of intravitreal injections are limited because invasive techniques are involved.[15,16]

In recent years, molecular imaging techniques have become a turning point for the development and pharmacokinetic study of new drugs. These techniques involve noninvasive procedures in order to significantly decrease the number of animals used by increasing the number of measurements on each animal.[17,18] In particular for the field of intravitreal drugs, single photon emission computed tomography and magnetic resonance image (MRI) have been the most commonly used imaging techniques, mainly to study pharmacokinetics[14,19] and the release of drugs from implants and liposomes.[20–22]

However, in pharmacokinetic studies performed with MRI, the molecules used for the labeling of the drug usually have very high molecular weight, which can alter the properties of the original drug.[21]

The use of positron emission tomography (PET) has made it possible to label drugs with small β-emitting radioisotopes.[23] Current integrated PET/computed tomography (CT) scanners allow visualization of radiolabeled molecules by using a direct and noninvasive methodology, and the follow-up of the same subject over time to determine the pharmacokinetic properties of intravitreal injections.[24–26]

Different radionuclides can be used to elaborate radiotracers for PET scanning. The most commonly used radionuclides are typically isotopes with short half-lives such as ^{11}C, ^{13}N, ^{15}O, ^{18}F, ^{68}Ga, ^{82}Rb, or with longer half-lives such as ^{124}I or ^{89}Zr. ^{18}F is one of the most widely used because it is easily produced with a cyclotron, its positron energy of emission is 0.64 MeV, it is safe for patients, and it allows to obtain images with high resolution. Moreover, its half-life is long enough to be able to produce commercially manufactured fluorinated radiotracers at off-site locations and to be shipped to imaging services. In practice, ^{18}F radionuclide is linked to different molecules to achieve selective transport and distribution.[27]

Drug clearance in the vitreous can be influenced by various factors that include molecular weight, physicochemical properties of the drug, surgical procedure, injected volumes, and presence of ocular inflammation.[1] Also, the mechanisms of membrane transport and plasmatic clearance can highly influence the distribution and elimination of drugs after intravitreal administration. For this reason, fluorodeoxyglucose (^{18}F-FDG), ^{18}F-choline (^{18}F-Choline), and ^{18}F–sodium fluoride (^{18}F-NaF) were selected in our study because of their different molecular weight, polarity, and transport mechanism across biological membranes. The aim of the present work was to study the effect of some of these factors on the vitreous clearance by using dedicated PET/CT imaging techniques for in vivo studies in rats.

Materials and Methods

Our work was designed as an experimental study in rats scanned in a dedicated PET/CT system after intravitreal injections of different radiolabeled molecules, different volumes, and absence/presence of inflammatory eye disease (uveitis).

Animals

This study was carried out on male adult Sprague Dawley rats with an average weight of 300 g, supplied by the animal facility of the University of Santiago de Compostela (Santiago de Compostela, Spain). During the experiments, the animals were kept in individual cages with free access to food and water in a room under controlled temperature (22°C ± 1°C) and humidity (60% ± 5%) and with day–night cycles regulated by artificial light (12/12 hours). The animals were treated as indicated in the ARVO Statement for the Use of Animals in Ophthalmic and Vision Research and according to the guidelines for laboratory animals.[28,29] Experiments were approved by the Galician Network Committee for Ethical Research and followed the Spanish and European Union (EU) rules (86/609/CEE, 2003/65/CE, 2010/63/EU, RD 1201/2005, and RD53/2013).

Intravitreal Injection Procedure

Intravitreal injection was performed according to the procedure described previously by Chiu et al.[30] Firstly, the animals were placed in a gas chamber containing 2% isoflurane in oxygen. When unconscious, the animals were removed from the chamber but kept under anesthesia with a mask (1.5% isoflurane in oxygen). The procedure was initiated by applying one drop of topical anesthesia (Colircusi Anestesico Doble: tetracaine 1 mg/mL and oxybuprocaine 4 mg/mL) on the eye followed by mydriatic eye drops (phenylephrine 100 mg/mL [Colircusi Fenilefrina] and tropicamide 10 mg/mL [Colircusi Tropicamide]) to visualize the eye fundus. Thereafter, radiolabeled molecules were injected into the vitreous through the pars plana by using a Hamilton syringe with a 34-G needle. The injection procedure was performed with a surgical microscope (Takagi OM-5 220-2; Takagi, Tokyo, Japan). Pictures of the procedure were taken by means of a digital camera (Nikon D-200; Nikon, Tokyo, Japan) attached to the microscope. Eyes with lens damage, or with significant bleeding when the intravitreal injection was made, were discarded from the study.

Experiments

The experiments were carried out by using intravitreal injections with three radiolabeled molecules and three different injection volumes, in healthy eyes and in eyes with lipopolysaccharide (LPS)–induced uveitis.

Effect of the Type of Injected Radiolabeled Molecules

Three different molecules were labeled with ^{18}F to evaluate the intravitreal pharmacokinetics. The radiolabeled molecules to be injected were ^{18}F-NaF, ^{18}F-FDG, and ^{18}F-Choline, with molecular weights of 41, 182, and 122 g/mol, respectively (Fig. 1).

The radioisotope $^{18}F^-$ was obtained from the nuclear reaction ^{18}O (proton, neutron) carried out in our PET Trace 800 cyclotron, according to the method described by Saha.[31] The radiosynthesis of ^{18}F-Na was made with a carbonate-type anion-exchange resin column, in such a way that the $^{18}F^-$ is retained into the column and it is recovered as ^{18}F–sodium

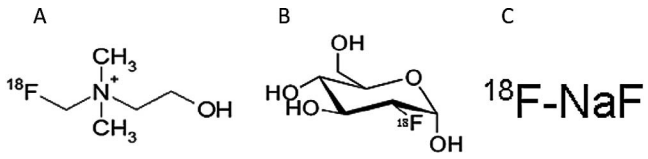

Figure 1. Chemical structure of (**A**) ^{18}F-Choline, (**B**) ^{18}F-FDG, and (**C**) ^{18}F-NaF.

fluoride by elution with potassium carbonate solution. ^{18}F-FDG and ^{18}F-Choline were produced on a TRACERlab MX synthesizer (GE Healthcare, Waukesah, WI, USA) by using cassettes and reagent kits from ABX (Advanced Biochemical Compounds, Radeberg, Germany). The nucleophilic substitution standard method was used in the case of ^{18}F-FDG and for the reaction of 18F-fluoromethyl triflate with dimethylethanolamine on a Sep-Pak column used in the case of ^{18}F-Choline.[32,33]

All procedures to obtain radiolabeled molecules were performed under good-manufacturing-practice conditions following the specific standards of European Pharmacopoeia.[34] The purity and stability quality control requirements were undertaken via high-pressure liquid chromatography/ion chromatography (930 Compact IC Flex con; Metrohm AG, Herisau, Switzerland) and thin layer chromatography. Osmolality (mOsm/kg) and pH were determined with a vapor pressure osmometer (VAPRO 5520; ELITECH Group, Paris, France) and a pH meter (WTW inoLab; WTW, Weilheim, Germany).

Effect of the Injected Volumes

The effect of the injected volume on the intravitreal pharmacokinetics of the abovementioned molecules was evaluated by using three different volumes: 2, 4, and 7 μL.

Effect of the Presence of Inflammation

Intravitreal pharmacokinetics was assessed in a uveitis animal model previously used by our group[33] and then compared to the intravitreal pharmacokinetics in healthy eyes. To induce uveitis, rats were inoculated into the right posterior paw with 1 mg/kg *Escherichia coli* LPS diluted in 0.1 mL phosphate-buffered saline by using a BD Micro-Fine syringe (BD, Oxford, UK) with 30-G needles. The presence of uveitis was assessed by direct inspection of the eye, using the surgical microscope. The animals were kept under such conditions for 24 hours. To reduce the number of animals, the influence of volume and presence or absence of uveitis were examined only for ^{18}F-NaF (monoexponential kinetics) and ^{18}F-FDG (biexponential kinetics). Four animals (eight eyes) were used in each condition studied.

Data Acquisition and Analysis

PET Data Acquisition. After the intravitreal injections of 1 MBq in each eye for all experimental conditions, dynamic PET acquisition was carried out to generate eight images of 15 minutes' duration for the first 1.5 hours. Afterwards, single PET images were obtained at 4 and 6 hours after drug administration. PET and CT images were acquired by using an Albira PET/CT Preclinical Imaging System (Bruker Biospin, Woodbridge, CT, USA). Animals were kept under anesthesia with a mask (1.5% isoflurane in oxygen). Respiration frequency and body temperature were monitored during the anesthesia period. The PET subsystem comprises three rings of eight compact modules based on monolithic crystals coupled to multianode photomultiplier tubes, forming an octagon with an axial field of view (FOV) of 40 mm per ring and a transaxial FOV of 80 mm in diameter. The CT system comprises a commercially available microfocus x-ray tube and a CsI scintillator 2D pixelated flat panel x-ray detector. Scatter and random coincidences were corrected by using the protocols implemented in the scanner. Attenuation correction was not performed. Images were reconstructed by using the maximum likelihood expectation maximization algorithm. Twelve iterations were performed with a reconstructed image pixel size of $0.4 \times 0.4 \times 0.4$ mm^3.

PET Data Analysis. After reconstruction, quantitative measurements were obtained by using the Amide's Medical Image Data Examiner.[35] Different regions of interest (ROIs) were manually drawn containing the signal on each eye. The ROIs were then replicated on the different temporal image frames to obtain the decrease curve of the radioisotope over time, conveniently corrected for radioactive decay.

Statistical Analysis. The curves of percentage of radiotracer in the eye versus time were fitted to the mono- and bicompartimental pharmacokinetic model by using nonlinear least squares regression analysis. The area under the percentage of radiotracer time curve AUC_0^{360} from zero to infinity was calculated by log-trapezoidal rule. The statistical analysis of experiments was performed by using a 1-way analysis of variance (ANOVA) and Tukey's multiple comparisons test. The nonlinear fitting and the statistical analysis were made by using the GraphPad Prism 6.0 software (2014; GraphPad Software, Inc., San Diego, CA, USA).

Results

All radiolabeled molecules were clearly detected in the vitreous cavity at the initial time of the study and it was possible to observe how the signal decreased over time. Figure 2 shows the coronal views of the fused PET/CT images from the initial frame (10 minutes after the injection) to the last frame (360 minutes after the injection).

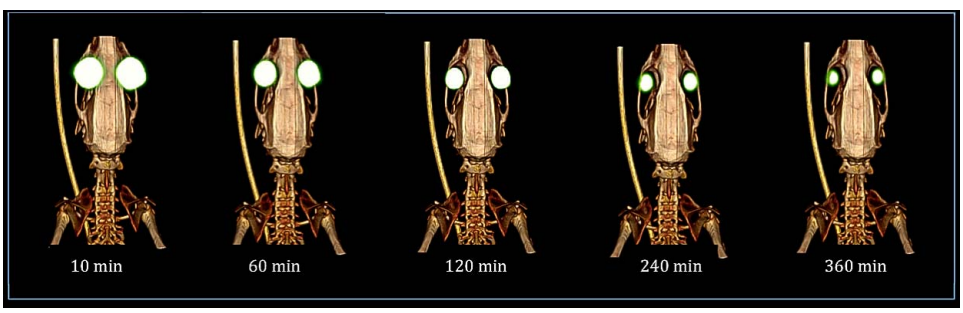

Figure 2. Fused image PET/CT showing the signal evolution in the rat eyes throughout time (minutes).

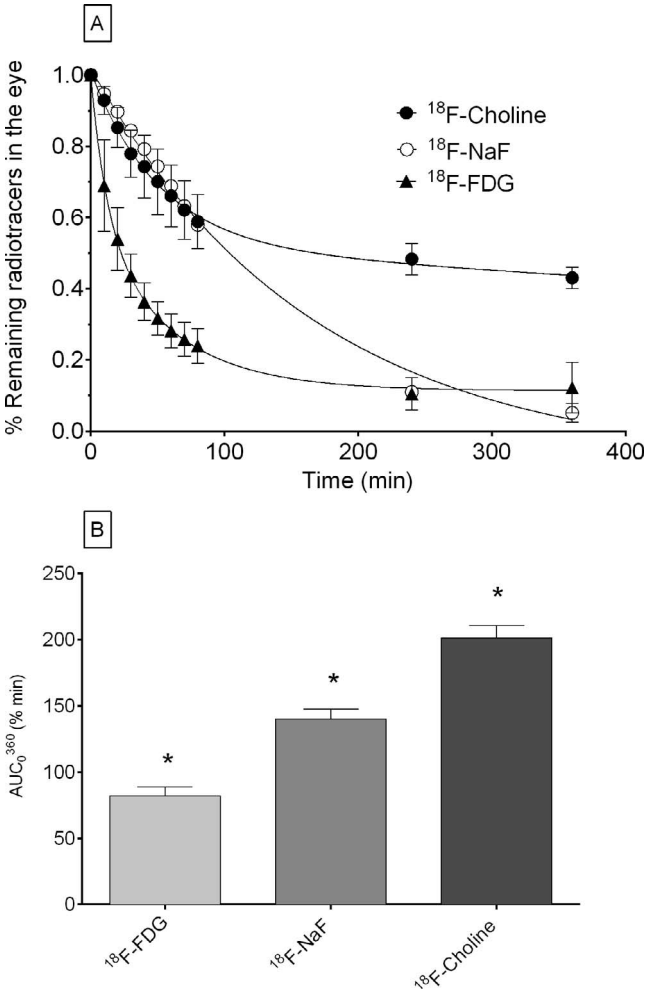

Figure 3. Influence of the drug type on its intravitreal release (mean ± SD, $n = 8$). (**A**) Intravitreal pharmacokinetic profile of ^{18}F-FDG, ^{18}F-NaF, and ^{18}F-Choline after intravitreal injection of 4 µL. (**B**) Representation of AUC_0^{360} (% min) for all radiotracers. *1-way ANOVA analysis and Tukey multiple comparison test show significant differences among the three different compounds ($\alpha < 0.01$).

Effect of the Type of Radiolabeled Molecules

The values measured from the ROI, containing each eye throughout time, were obtained for the three radiolabeled molecules, giving rise to significantly different kinetic curves (Fig. 3A). On the one hand, the clearance curves from ^{18}F-FDG and ^{18}F-Choline tracers appeared to fit a two-compartment model with a biphasic clearance from the vitreous. The obtained average intravitreal half-lives for these radiolabeled molecules were13.99 minutes for ^{18}F-FDG and 35.18 minutes for ^{18}F-Choline for the initial rapid elimination phase (α), and 214.2 minutes and 1351 minutes, respectively, for the slow elimination phase (β). Table 1 shows the pharmacokinetic parameters obtained by fitting the data to a bicompartmental model. On the other hand, the clearance curve from ^{18}F-Na showed a one-compartment pharmacokinetic model, and the average intravitreal half-life was 113.2 minutes. Table 2 shows the pharmacokinetic parameters obtained by fitting the data to a one-compartment pharmacokinetic model.

When comparing the area under the curve between 0 and 360 minutes (AUC_0^{360}) among three radiolabeled molecules, it was observed that ^{18}F-Choline remains significantly longer in the eye than ^{18}F-FDG and ^{18}F-NaF (Fig. 3B).

The radiolabeled molecules leave the eye and reach the systemic circulation, following different kinetic curves. Furthermore, the distribution at system level is also significantly different. Figure 4 shows that ^{18}F-NaF is captured by bone structures, while ^{18}F-FDG and ^{18}F-Choline are captured by internal organs.

The radiolabeled molecules used for the intravitreal injection had radiochemical purity for ^{18}F-FDG higher than 95% with a specific activity of approximately 1000 MBq/mL. The ^{18}F-Choline had radiochemical purity higher than 95% with a specific activity of approximately 500 MBq/mL. All radiotracers showed percentages of fluorine bound to the radiotracer that were higher than 95% at 8 hours post synthesis. The osmolality of all radiolabeled solutions was approximately 280 ± 10 mOsm/kg with a pH ≈7.4.

Effect of the Injected Volumes

Figure 5 shows no differences between the different volumes of intravitreal injections (2, 4, and 7 µL) for ^{18}F-Na and ^{18}F-FDG radioisotopes, which follow the same kinetics as previously described in Figure 3A. Tables 1 and 2 show that no statistically significant differences were found between pharmacokinetic parameters in relation to the injected volumes of both ^{18}F-FDG (Table 1) and ^{18}F-Na (Table 2). Finally, it should be noted that a transient vascular collapse in the retinal vessels was observed after administration of 7 µL, but not for 2 and 4 µL.

Effect of the Presence of Inflammation

Figure 6A shows that inflammation slightly, but with statistical significance, increased the vitreous clearance of ^{18}F-FDG. This effect was quantified by comparing the AUC_0^{360} of radiolabeled molecules in uveitis and under normal conditions. Figure 6B

Table 1. Pharmacokinetic Parameters Obtained by Fitting the Data to a Bicompartmental Model for ^{18}F-FDG and ^{18}F-Choline

	^{18}F-FDG				^{18}F-Choline
		4 µL*			
Pharmacokinetic Parameters	**2 µL***	**Normal†**	**Uveitis†**	**7 µL***	**7 µL**
α, min^{-1}	0.0336	0.03341	0.0416	0.0495	0.01970
$t_{1/2\alpha}$, min	20.65	20.75	16.66	13.99	35.18
B, min^{-1}	0.00285	0.002421	0.00218	0.00324	0.00051
$t_{1/2\beta}$, min	243.0	286.4	317.8	214.2	1351
AUC_0^{360}, % min	70.13 ± 5.31	88.15 ± 7.86	70.01 ± 5.70	82.05 ± 15.67	201.3 ± 18.83
R^2	0.9958	0.9958	0.9938	0.9963	0.9971

* No statistical differences for AUC_0^{360} (% min) were observed between different injection volumes (α not significant [n.s.]).
† Statistical differences for AUC_0^{360} (% min) between normal and uveitis eyes for $\alpha < 0.01$.

Table 2. Pharmacokinetic Parameters Obtained by Fitting the Data to Monocompartmental Model With ^{18}F-NaF

	^{18}F-NaF			
		4 µL*		
Pharmacokinetic Parameters	**2 µL***	**Normal†**	**Uveitis†**	**7 µL***
k, min^{-1}	0.00669	0.00656	0.00805	0.00612
$t_{1/2}$, min	103.6	105.7	86.11	113.2
AUC_0^{360}, % min	140.15 ± 14.93	135.23 ± 14.09	123.69 ± 21.09	137.03 ± 5.72
R^2	0.9982	0.9982	0.9952	0.9956

* No statistical differences were observed for AUC_0^{360} (% min) between different injection volumes (α n.s.).
† No statistical differences were observed for AUC_0^{360} (% min) between normal and uveitis eyes (α n.s.).

shows that eyes with uveitis had smaller AUC_0^{360} than normal eyes. In addition, statistically significant differences were found between the pharmacokinetic parameters in uveitis and normal conditions for the case of ^{18}F-FDG (Table 1). It must be mentioned that animals receiving an LPS injection developed a fibrinous reaction in the anterior chamber of the eye, which produced a pupillary membrane and an irregular pupil after drug-induced mydriasis, caused by the adhesion of the iris to the lens (Fig. 7). The uveitis model was successfully achieved in the same way as obtained in our previous studies.[36]

Discussion

Intravitreal injections are increasingly used in a multitude of retinal ophthalmic conditions such as age-related macular degeneration,[37] diabetic macular edema,[38] macular holes,[39] branch and central retinal vein occlusion,[40] and endophthalmitis.[41] The development of new intravitreal drugs or systems that modify their release involves wide preclinical development[42] in which pharmacokinetic studies play a key role.[43]

The use of small animals, such as Sprague Dawley rats, has many advantages because of their small size, the availability of research animal facilities, and multiple disease models suitable for them.[44,45] However, since they have a small vitreous volume, classic pharmacokinetic studies become difficult, with in vivo imaging being an ideal technique, as no invasive modalities are required to obtain experimental results.[46,47] To the best of our knowledge, our work is the first study of intravitreal pharmacokinetics with PET/CT in rats. Previous intravitreal pharmacokinetic studies have required larger

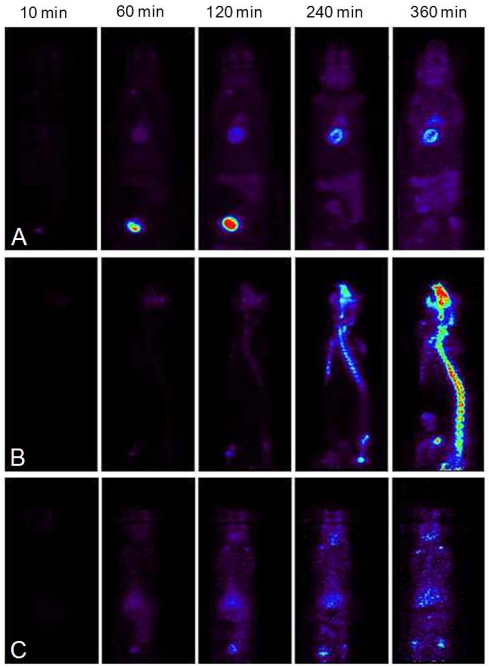

Figure 4. Representation of the systemic distribution of radiotracers at different times after intravitreal administration. (**A**) Coronal views after injection of ^{18}F-FDG. (**B**) Sagittal views after injection of ^{18}F-NaF. (**C**) Coronal views after injection of ^{18}F-Choline.

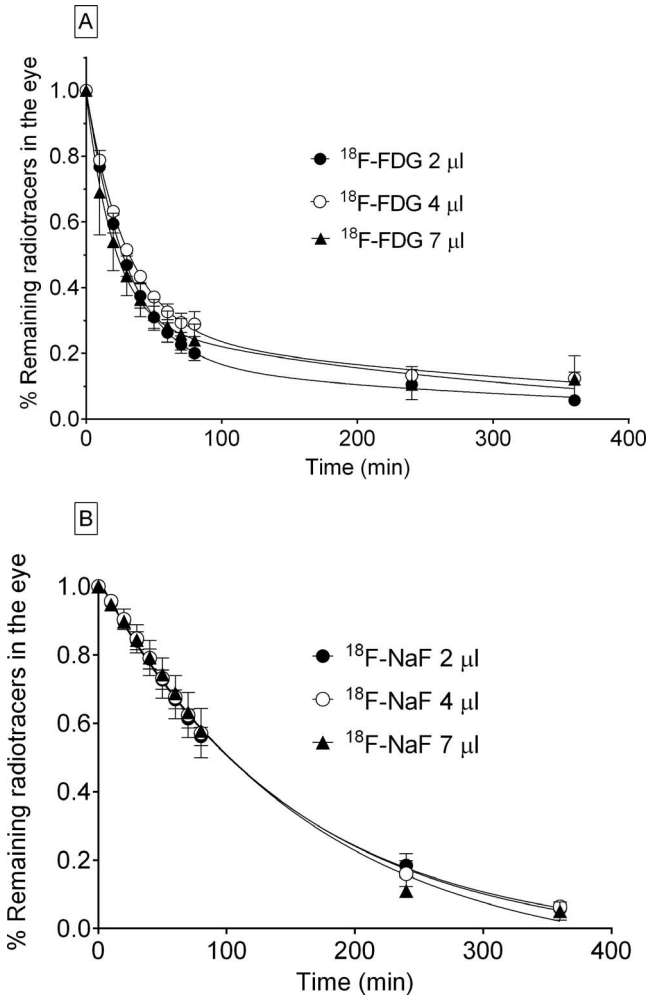

Figure 5. Influence of the injection volume on vitreal release (mean ± SD, $n = 8$). Intravitreal pharmacokinetic profile of ^{18}F-FDG (**A**) and ^{18}F-NaF (**B**) after intravitreal injection of 2, 4, and 7 µL.

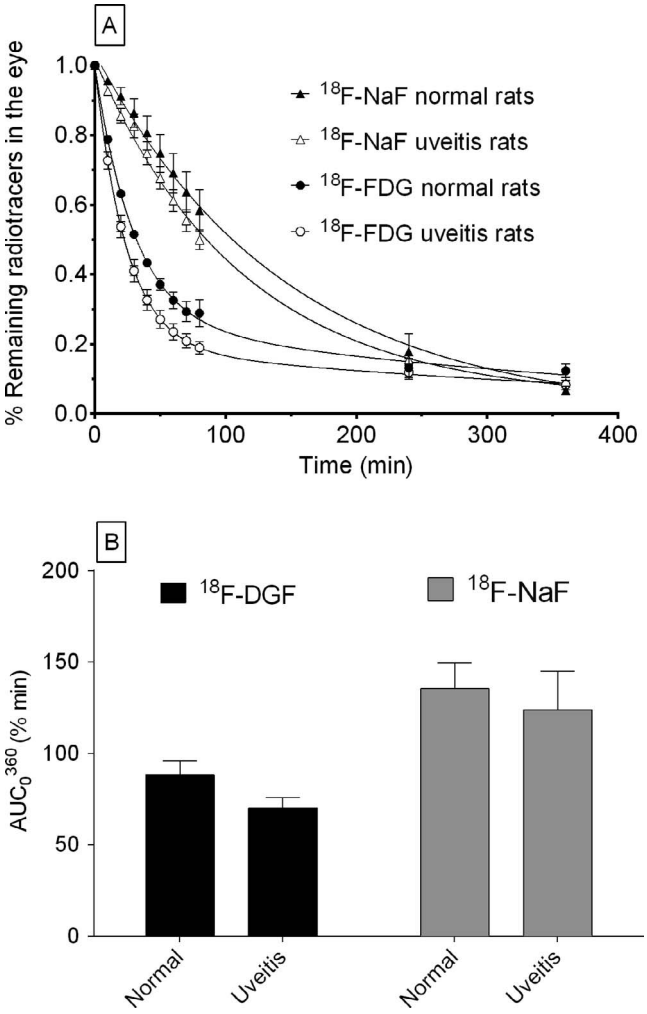

FIGURE 6. Influence of inflammation on vitreal release (mean ± SD, $n = 8$). (**A**) Intravitreal pharmacokinetic profile of ^{18}F-FDG and ^{18}F-NaF after a 7-μL intravitreal injection in normal eyes and in eyes with uveitis. (**B**) Representation of AUC_0^{360} (% min) for ^{18}F-FDG and ^{18}F-NaF in these conditions. *Statistical significant differences between normal and uveitis eyes for $\alpha < 0.01$.

numbers of animals and more complex techniques to determine vitreous drug levels at different time points.[48–50] In our study serial measurements were obtained at multiple time points after the intravitreal injection in the same animal. The advantage of preclinical PET/CT images in this field is very important because the technique is noninvasive, and it yields images in 3D and real time.[51] PET/CT is also becoming a relevant procedure for ophthalmic research, as it has been used for diagnosis of intraocular tumors,[52] neurophysiological studies,[53,54] or pharmacokinetic studies with topical ophthalmic formulations.[23] Although PET is a very sensitive technique, it presents some limitations related to low spatial resolution. As an example, the delineation of the vitreous area is troublesome and challenging owing to the small size of the eyeball, and therefore our measurements cannot be restricted exclusively to the vitreous area.

More than 10% of currently used drugs contain fluorine atoms that can be labeled with ^{18}F. Moreover, the substitution of oxygen atoms or hydroxyl groups by fluorine is relatively easy with no critical changes in the properties of the molecule.[55] Fluoride and oxygen have a very similar radius, whereas that of hydrogen is slightly smaller (van der Waals radii

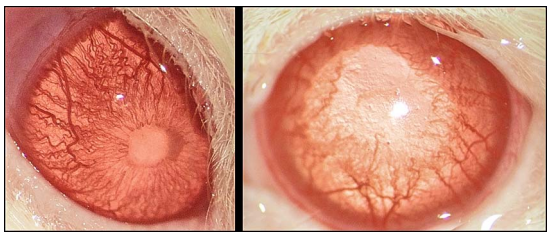

FIGURE 7. Anterior segment of two eyes 24 hours after pad injection of LPS, showing signs of uveitis. *Left*: Fibrinous reaction producing a pupillary membrane. *Right*: Irregular pupil after drug-induced mydriasis caused by the adhesion of the iris to the lens.

are 1.47, 1.57, and 1.20 angstroms, respectively); therefore, changing oxygen or hydrogen for fluoride does not entail substantial modifications in the molecular structure by steric impediments. Furthermore, in terms of Taft E_s parameters,[56] fluoride and hydroxyl substituents have very similar characteristics (+0.78 vs. +0.69); therefore, their substitution does not compromise either the structural activity of the compound or its interaction with receptors. The electronegativity of fluoride and hydrogen atoms is different (4.0 vs. 2.1), hence interchanging them can substantially affect the physicochemical properties of the molecule (pKa, hydrogen bond capacity, or lipophilicity). On the contrary, fluoride and oxygen have similar values (4.0 vs. 3.5), so no major changes should be expected when interchanged.[55] Owing to the relatively short half-life of ^{18}F, the fluorinated radiotracers have limited use in studies of pharmacokinetics or biodistribution of drugs with long half-lives in the vitreous cavity. For these long-term studies, using other radiotracers with long half-lifes such as ^{124}I (Kuntner et al.[57] and Dangl et al.[58]) or ^{89}Zr (Van Loon et al.[59]) is more adequate.

Fluorinated radiotracers, as the ones used in this work, have the advantage of their low positron emission energy (the lowest of all the radiolabels used in PET). Furthermore, the greater sensitivity of modern PET technology allows the use of low radioactivity levels, so the dose received and absorbed by the animal is significantly below the dose limit.[60] Additionally, during the disintegration of ^{18}F, no γ rays or α and β particles are emitted, reducing the dose received by animals and increasing safety.[61] On the other hand, cytotoxicity and acute irritation of fluorinated radiotracers have been described as safe in previous reports.[23] In our study, no alterations in the eye of the animals were observed after the administration of the fluorinated radiotracers.

Our findings showed significant differences between the different radiolabeled molecules we used. The reason for these differences could rest on the mechanism used for crossing the BRB. In the rat retina there are transporters for glucose and cationic amino acids, which probably are used by ^{18}F-FDG and ^{18}F-Choline to leave the vitreous cavity.[62] The biexponential kinetics we observed is also common for intravitreal drugs such as bevacizumab and ranibizumab.[50,63] Furthermore, it must be mentioned that hyaluronic acid, which is part of the vitreous humor, has a highly negative charge at physiological pH levels. Because of this, it could interact with positively charged molecules, such as choline, by generating polyelectrolyte complexes with low solubility.[64] This is probably the reason why choline is released at a slower rate than glucose. On the other hand, our findings showed that ^{18}F-NaF is eliminated from the vitreous, following monoexponential kinetics, which could be explained by assuming passive diffusion through the BRB because this compound diffuses freely across membranes.[65] It would be similar to the release kinetics of other intravitreal drugs, such as aflibercept.[66,67]

Our findings showed that the injected volume had no significant influence on vitreous drug clearance. Different studies have been carried out in human eyes[68] and in murine models[69,70] using a wide range of intravitreal injection volumes (2–20 μL), but they did not include an evaluation of their impact on the vitreous drug clearance. On the other hand, it has been pointed out that an increase of intraocular pressure could result in an increase of hydraulic flow, derived from the excess of volume introduced.[10] This increase in intraocular pressure could be the cause of the transitory collapse we observed with the administration of 7 μL. However, this process seems not to have an effect on the vitreous clearance of low-molecular-weight drugs,[71,72] such as the ones we used, where all radiolabeled molecules had molecular weights below 500 Da. Finally, it has to be mentioned that the vitreous volume of a rat is smaller than that of humans (approximately 50 μL in rats versus 4.5 mL in humans)[73] (Vezina M, et al. *IOVS* 2011;52:ARVO E-Abstract 3219). This difference must be kept in mind if our results are to be translated to humans.

Our results showed an increase in the intravitreal clearance of the ^{18}F-FDG radiotracer in eyes with inflammation (uveitis) when compared to healthy eyes. On the contrary, no significant differences were observed for ^{18}F-NaF. Studies using MRI techniques have shown that inflammation in rabbit eyes, induced by LPS, can increase the permeability of BRB.[74,75] On the other hand, additional studies have demonstrated that in inflammatory conditions, as in tumors, a high FDG uptake and a high GLUT-1 expression level is observed.[76] Of note, ^{18}F-NaF is not affected by changes produced by the inflammatory process probably because it is freely diffusible across membranes.[65] However, the increase in permeability and GLUT transporter under inflammatory conditions can increase the clearance of ^{18}F-FDG from the vitreous. Since the magnitude of the clearance changes we found were small, it would be necessary to carry out additional studies to properly establish the influence of inflammation on the BRB permeability. It is possible that the severity of the inflammatory process determines the increase of BRB permeability and hence, the intravitreal clearance rate.

Finally, although the effect of inhaled anesthesia, in particular isoflurane, on drug permeability has been extensively studied in the blood–brain barrier (BBB), no studies have shown any type of modification in the status of the BRB.[77] Inhaled isoflurane in rats decreases the transfer of small hydrophilic molecules across the BBB, either by reducing the perfused capillary surface area or by a direct effect of isoflurane on the permeability of the BBB.[78]

Even though BRB and BBB are thought to have similar properties owing to their similar anatomic features, some differences in the capillary endothelia at BBB and BRB have been found.[79] These differences could cause a variation in the permeability across BRB compared to BBB,[80] which would ultimately affect the half-life and clearance of drugs injected into the vitreous. Therefore, we cannot assume that the observed increase in permeability through BBB would lead to a similar effect in BRB. Studies about the effect on inhaled anesthesia on BRB permeability would be of great interest.

Conclusions

In summary, we demonstrated for the first time the usefulness of a PET-based methodology for the study of different factors influencing intravitreal pharmacokinetics in rats. This can be a powerful tool to develop new drugs aimed at treating ocular conditions, using intravitreal administration.

Acknowledgments

Supported by Instituto de Salud Carlos III Rio Hortega Research Grant CM15/00188 (AF-F) and Miguel Servet Research Grant CP12/03162 (JP-M), MICINN Ramon y Cajal RYC-2015-17430 (PA), and partially supported by the government research funding agencies of Xunta de Galicia, Spain (ED431C-2016-025, ED341D-R2016-032), and by ISCIII (RETICS Oftared, RD16/0008/0003 and RD12/0034/0017) cofunded by FEDER.

Disclosure: **A. Fernández-Ferreiro**, None; **A. Luaces-Rodríguez**, None; **P. Aguiar**, None; **J. Pardo-Montero**, None; **M. González-Barcia**, None; **L. García-Varela**, None; **M. Herranz**, None; **J. Silva-Rodríguez**, None; **M. Gil-Martínez**, None; **M.A. Bermúdez**, None; **A. Vieites-Prado**, None; **J. Blanco-Méndez**, None; **M.J. Lamas**, None; **F. Gómez-Ulla**, None; **Á. Ruibal**, None; **F.J. Otero-Espinar**, None; **F. González**, None

References

1. Radhika M, Mithal K, Bawdekar A, et al. Pharmacokinetics of intravitreal antibiotics in endophthalmitis. *J Ophthalmic Inflamm Infect*. 2014;4:22.
2. Fernández-Ferreiro A, Silva-Rodríguez J, Otero-Espinar FJ, et al. In vivo eye surface residence determination by high-resolution scintigraphy of a novel ion-sensitive hydrogel based on gellan gum and kappa-carrageenan. *Eur J Pharm Biopharm*. 2017;114:317–323.
3. Fernández-Ferreiro A, González-Barcia M, Otero Espinar FJ, Blanco Méndez J, Lamas MJ. Ophthalmic formulations new goals [in Spanish]. *Farm Hosp*. 2016;40:1–2.
4. Gaudana R, Ananthula HK, Parenky A, Mitra AK. Ocular drug delivery. *AAPS J*. 2010;12:348–360.
5. Solomon SD, Lindsley K, Vedula SS, Krzystolik MG, Hawkins BS. Anti-vascular endothelial growth factor for neovascular age-related macular degeneration. *Cochrane Database Syst Rev*. 2014;8:CD005139.
6. Balachandran RK, Barocas VH. Computer modeling of drug delivery to the posterior eye: effect of active transport and loss to choroidal blood flow. *Pharm Res*. 2008;25:2685–2696.
7. Awwad S, Lockwood A, Brocchini S, Khaw PT. The PK-Eye: a novel in vitro ocular flow model for use in preclinical drug development. *J Pharm Sci*. 2015;104:3330–3342.
8. Park J, Bungay PM, Lutz RJ, et al. Evaluation of coupled convective–diffusive transport of drugs administered by intravitreal injection and controlled release implant. *J Control Release*. 2005;105:279–295.
9. Krishnamoorthy MK, Park J, Augsburger JJ, Banerjee RK. Effect of retinal permeability, diffusivity, and aqueous humor hydrodynamics on pharmacokinetics of drugs in the eye. *J Ocul Pharmacol Ther*. 2008;24:255–267.
10. Xu J, Heys JJ, Barocas VH, Randolph TW. Permeability and diffusion in vitreous humor: implications for drug delivery. *Pharm Res*. 2000;17:664–669.
11. Gisladottir S, Loftsson T, Stefansson E. Diffusion characteristics of vitreous humour and saline solution follow the Stokes Einstein equation. *Graefes Arch Clin Exp Ophthalmol*. 2009;247:1677–1684.
12. Ohtori A, Tojo K. In vivo/in vitro correlation of intravitreal delivery of drugs with the help of computer simulation. *Biol Pharm Bull*. 1994;17:283–290.
13. Tojo K, Nakagawa K, Morita Y, Ohtori A. A pharmacokinetic model of intravitreal delivery of ganciclovir. *Eur J Pharm Biopharm*. 1999;47:99–104.
14. Del Amo EM, Rimpelä A-K, Heikkinen E, et al. Pharmacokinetic aspects of retinal drug delivery. *Prog Retin Eye Res*. 2017;57:134–185.
15. Avery RL, Castellarin AA, Steinle NC, et al. Systemic pharmacokinetics following intravitreal injections of ranibi-

zumab, bevacizumab or aflibercept in patients with neovascular AMD. *Br J Ophthalmol*. 2014;98:1636–1641.

16. Bhagat R, Zhang J, Farooq S, Li X-Y. Comparison of the release profile and pharmacokinetics of intact and fragmented dexamethasone intravitreal implants in rabbit eyes. *J Ocul Pharmacol Ther*. 2014;30:854–858.
17. Cunha L, Szigeti K, Mathé D, Metello LF. The role of molecular imaging in modern drug development. *Drug Discov Today*. 2014;19:936–948.
18. Capozzi ME, Gordon AY, Penn JS, Jayagopal A. Molecular imaging of retinal disease. *J Ocul Pharmacol Ther*. 2013;29:275–286.
19. Rimpelä A-K, Schmitt M, Latonen S, et al. Drug distribution to retinal pigment epithelium: studies on melanin binding, cellular kinetics, and single photon emission computed tomography/computed tomography imaging. *Mol Pharm*. 2016;13:2977–2986.
20. Li SK, Lizak MJ, Jeong E-K. MRI in ocular drug delivery. *NMR Biomed*. 2008;2:941–956.
21. Kim H, Lizak MJ, Tansey G, et al. Study of ocular transport of drugs released from an intravitreal implant using magnetic resonance imaging. *Ann Biomed Eng*. 2005;33:150–164.
22. Molokhia SA, Jeong E-K, Higuchi WI, Li SK. Transscleral iontophoretic and intravitreal delivery of a macromolecule: study of ocular distribution in vivo and postmortem with MRI. *Exp Eye Res*. 2009;88:418–425.
23. Fernández-Ferreiro A, Silva-Rodríguez J, Otero-Espinar FJ, et al. Positron emission tomography for the development and characterization of corneal permanence of ophthalmic pharmaceutical formulations. *Invest Ophthalmol Vis Sci*. 2017;58:772–780.
24. Christoforidis JB, Williams MM, Kothandaraman S, Kumar K, Epitropoulos FJ, Knopp MV. Pharmacokinetic properties of intravitreal I-124-aflibercept in a rabbit model using PET/CT. *Curr Eye Res*. 2012;37:1171–1174.
25. Christoforidis JB, Carlton MM, Knopp MV, Hinkle GH. PET/CT imaging of I-124-radiolabeled bevacizumab and ranibizumab after intravitreal injection in a rabbit model. *Invest Ophthalmol Vis Sci*. 2011;52:5899–5903.
26. Christoforidis JB, Williams MM, Wang J, et al. Anatomic and pharmacokinetic properties of intravitreal bevacizumab and ranibizumab after vitrectomy and lensectomy. *Retina*. 2013;33:946–952.
27. Okamura N, Harada R, Furukawa K, et al. Advances in the development of tau PET radiotracers and their clinical applications. *Ageing Res Rev*. 2016;30:107–113.
28. The Association for Research in Vision and Ophthalmology. Statement for the Use of Animals in Ophthalmic and Visual Research. Available at: http://www.arvo.org/About_ARVO/Policies/Statement_for_the_Use_of_Animals_in_Ophthalmic_and_Visual_Research/. Published November 28, 2014. Accessed October 3, 2016.
29. National Research Council (US) Committee for the Update of the Guide for the Care and Use of Laboratory Animals. *Guide for the Care and Use of Laboratory Animals*. 8th ed. Washington, DC: National Academies Press; 2011. Available at: http://www.ncbi.nlm.nih.gov/books/NBK54050/. Accessed November 28, 2014.
30. Chiu K, Chang RC-C, So K-F. Intravitreous injection for establishing ocular diseases model. *J Vis Exp*. 2007;8:313.
31. Saha B. *Basics of PET Imaging: Physics, Chemistry, and Regulations*. New York: Springer-Verlag; 2010.
32. Yu S. Review of 18F-FDG synthesis and quality control. *Biomed Imaging Interv J*. 2006;2:e57.
33. Vallabhajosula S. *Molecular Imaging: Radiopharmaceuticals for PET and SPECT*. New York: Springer-Verlag; 2009.
34. The European Pharmacopoeia Commision. *European Pharmacopoeia*. Available at: https://www.edqm.eu/en/european-pharmacopoeia-commission.
35. Loening AM, Gambhir SS. AMIDE: a free software tool for multimodality medical image analysis. *Mol Imaging*. 2003;2:131–137
36. Bermudez MA, Sendon-Lago J, Seoane S, et al. Anti-inflammatory effect of conditioned medium from human uterine cervical stem cells in uveitis. *Exp Eye Res*. 2016;149:84–92.
37. Lindsley K, Li T, Ssemanda E, Virgili G, Dickersin K. Interventions for age-related macular degeneration: are practice guidelines based on systematic reviews? *Ophthalmology*. 2016;123:884–897.
38. Payne JF, Wykoff CC, Clark WL, Bruce BB, Boyer DS, Brown DM. Randomized trial of treat and extend ranibizumab with and without navigated laser for diabetic macular edema: TREX-DME 1 year outcomes. *Ophthalmology*. 2017;124:74–81.
39. Bennison C, Stephens S, Lescrauwaet B, Van Hout B, Jackson TL. Cost-effectiveness of ocriplasmin for the treatment of vitreomacular traction and macular hole. *J Mark Access Health Policy*. 2016;4:31472.
40. Clark WL, Boyer DS, Heier JS, et al. Intravitreal aflibercept for macular edema following branch retinal vein occlusion: 52-week results of the VIBRANT Study. *Ophthalmology*. 2016;123:330–336.
41. Joseph J, Nirmalkar K, Mathai A, Sharma S. Clinical features, microbiological profile and treatment outcome of patients with Corynebacterium endophthalmitis: review of a decade from a tertiary eye care centre in southern India. *Br J Ophthalmol*. 2016;100:189–194.
42. Martens TF, Remaut K, Deschout H, et al. Coating nanocarriers with hyaluronic acid facilitates intravitreal drug delivery for retinal gene therapy. *J Control Release*. 2015;202:83–92.
43. Adamson P, Wilde T, Dobrzynski E, et al. Single ocular injection of a sustained-release anti-VEGF delivers 6 months pharmacokinetics and efficacy in a primate laser CNV model. *J Control Release*. 2016;244(part A):1–13.
44. Williams D. Rabbit and rodent ophthalmology. *Eur J Companion Anim Pract*. 2007;17:242–252.
45. Pennesi ME, Neuringer M, Courtney RJ. Animal models of age related macular degeneration. *Mol Aspects Med*. 2012;33:487–509.
46. Willmann JK, van Bruggen N, Dinkelborg LM, Gambhir SS. Molecular imaging in drug development. *Nat Rev Drug Discov*. 2008;7:591–607.
47. Robinson MR, Baffi J, Yuan P, et al. Safety and pharmacokinetics of intravitreal 2-methoxyestradiol implants in normal rabbit and pharmacodynamics in a rat model of choroidal neovascularization. *Exp Eye Res*. 2002;74:309–317.
48. Gasparin F, Aguiar RG, Ioshimoto GL, et al. Pharmacokinetics, electrophysiological, and morphological effects of the intravitreal injection of mycophenolic acid in rabbits. *J Ocul Pharmacol Ther*. 2014;30:502–511.
49. Park SJ, Oh J, Kim Y-K, et al. Intraocular pharmacokinetics of intravitreal vascular endothelial growth factor-Trap in a rabbit model. *Eye (Lond)*. 2015;29:561–568.
50. Bakri SJ, Snyder MR, Reid JM, Pulido JS, Singh RJ. Pharmacokinetics of intravitreal bevacizumab (Avastin). *Ophthalmology*. 2007;114:855–859.
51. Kuntner C, Stout DB. Quantitative preclinical PET imaging: opportunities and challenges. *Front Phys*. 2014;2:12
52. Sek K, Wilson D, Paton K, Benard F. The role of 18F-FDG PET/CT in assessment of uveal melanoma and likelihood of primary tumour visualisation based on AJCC tumour size. *J Nucl Med*. 2016;57:409–409.

Investigative Ophthalmology & Visual Science

53. García-Rojas L, Adame-Ocampo G, Alexánderson E, Tovilla-Canales JL. 18-fluorodeoxyglucose uptake by positron emission tomography in extraocular muscles of patients with and without Graves' ophthalmology. *J Ophthalmol*. 2013;2013: 529187.
54. Wang W-F, Ishiwata K, Kiyosawa M, et al. Investigation of the use of positron emission tomography for neuroreceptor imaging in rabbit eyes. *Ophthalmic Res*. 2004;36:255–263.
55. Amii H, Uneyama K. C–F bond activation in organic synthesis. *Chem Rev*. 2009;109:2119–2183.
56. Chambers RD. The influence of fluorine of fluorocarbon groups on some reaction centers. In: *Fluorine in Organic Chemistry*. Boca Raton, Florida: CRC Press; 2004.
57. Kuntner C, Wanek T, Hoffer M, et al. Radiosynthesis and assessment of ocular pharmacokinetics of 124I-labeled chitosan in rabbits using small-animal PET. *Mol Imaging Biol*. 2011;13:222–226.
58. Dangl D, Hornof M, Hoffer M, Kuntner C, Wanek T, Kvaternik H. In vivo evaluation of ocular residence time of 124i-labelled thiolated chitosan in rabbits using microPET technology. *Invest Ophthalmol Vis Sci*. 2009;50:3689–3689.
59. Van Loon J, Even AJG, Aerts HJWL, et al. PET imaging of zirconium-89 labelled cetuximab: a phase I trial in patients with head and neck and lung cancer. *Radiother Oncol*. 2017; 122:267–273.
60. Ainsbury EA, Bouffler SD, Dörr W, et al. Radiation cataractogenesis: a review of recent studies. *Radiat Res*. 2009;172:1–9.
61. Peñuelas Sánchez I. PET radiopharmaceuticals. *Rev Esp Med Nucl*. 2001;20:477–498.
62. Tombran-Tink J, Barnstable CJ. *Ocular Transporters in Ophthalmic Diseases and Drug Delivery*. Totowa, New Jersey: Humana Press; 2008.
63. Bakri SJ, Snyder MR, Reid JM, Pulido JS, Ezzat MK, Singh RJ. Pharmacokinetics of intravitreal ranibizumab (Lucentis). *Ophthalmology*. 2007;114:2179–2182.
64. Koss MJ, Hoffmann J, Nguyen N, et al. Proteomics of vitreous humor of patients with exudative age-related macular degeneration. *PLoS One*. 2014;9:e96895.
65. Czernin J, Satyamurthy N, Schiepers C. Molecular mechanisms of bone 18F-NaF deposition. *J Nucl Med*. 2010;51:1826–1829.
66. Thai H-T, Veyrat-Follet C, Vivier N, et al. A mechanism-based model for the population pharmacokinetics of free and bound aflibercept in healthy subjects. *Br J Clin Pharmacol*. 2011;72: 402–414.
67. Avery RL, Castellarin AA, Steinle NC, et al. Systemic pharmacokinetics and pharmacodynamics of intravitreal aflibercept, bevacizumab, and ranibizumab [published online ahead of print January 18, 2017]. *Retina*. doi:10.1097/IAE.0000000000001493.
68. Friedrich S, Saville B, Cheng YL. Drug distribution in the vitreous humor of the human eye: the effects of aphakia and changes in retinal permeability and vitreous diffusivity. *J Ocul Pharmacol Ther*. 1997;13:445–459.
69. Grant CA, Ponnazhagan S, Wang XS, Srivastava A, Li T. Evaluation of recombinant adeno-associated virus as a gene transfer vector for the retina. *Curr Eye Res*. 1997;16:949–956.
70. Li T, Davidson BL. Phenotype correction in retinal pigment epithelium in murine mucopolysaccharidosis VII by adenovirus-mediated gene transfer. *Proc Natl Acad Sci U S A*. 1995; 92:7700–7704.
71. Missel PJ. Hydraulic flow and vascular clearance influences on intravitreal drug delivery. *Pharm Res*. 2002;19:1636–1647.
72. Missel PJ. Finite and infinitesimal representations of the vasculature: ocular drug clearance by vascular and hydraulic effects. *Ann Biomed Eng*. 2002;30:1128–1139.
73. Basile AS, Glazier G, Lee A, et al. Intravitreal concentrations of a near-infrared fluorescence-labeled biotherapeutic determined in situ using confocal scanning laser ophthalmoscopy. *Invest Ophthalmol Vis Sci*. 2011;52:6949–6958.
74. Berkowitz BA, Roberts R, Luan H, Peysakhov J, Mao X, Thomas KA. Dynamic contrast-enhanced MRI measurements of passive permeability through blood retinal barrier in diabetic rats. *Invest Ophthalmol Vis Sci*. 2004;45:2391–2398.
75. Metrikin DC, Wilson CA, Berkowitz BA, Lam MK, Wood GK, Peshock RM. Measurement of blood-retinal barrier breakdown in endotoxin-induced endophthalmitis. *Invest Ophthalmol Vis Sci*. 1995;36:1361–1370.
76. Mochizuki T, Tsukamoto E, Kuge Y, et al. FDG uptake and glucose transporter subtype expressions in experimental tumor and inflammation models. *J Nucl Med*. 2001;42: 1551–1555.
77. Cheng Y, He L, Prasad V, Wang S, Levy RJ. Anesthesia-induced neuronal apoptosis in the developing retina: a window of opportunity. *Anesth Analg*. 2015;121:1325–1335.
78. Chi OZ, Anwar M, Sinha AK, Wei HM, Klein SL, Weiss HR. Effects of isoflurane on transport across the blood-brain barrier. *Anesthesiology*. 1992;76:426–431.
79. Stewart PA, Tuor UI. Blood-eye barriers in the rat: correlation of ultrastructure with function. *J Comp Neurol*. 1994;340: 566–576.
80. Toda R, Kawazu K, Oyabu M, Miyazaki T, Kiuchi Y. Comparison of drug permeabilities across the blood-retinal barrier, blood-aqueous humor barrier, and blood-brain barrier. *J Pharm Sci*. 2011;100:3904–3911.

Investigative Ophthalmology & Visual Science